

# Defects, disorder and strong electron correlations in orbital degenerate, doped Mott insulators

Adolfo Avella,<sup>1,2,3</sup> Andrzej M. Oleś,<sup>4,5</sup> and Peter Horsch<sup>4</sup>

<sup>1</sup>*Dipartimento di Fisica "E.R. Caianiello", Università degli Studi di Salerno, I-84084 Fisciano (SA), Italy*

<sup>2</sup>*CNR-SPIN, UoS di Salerno, I-84084 Fisciano (SA), Italy*

<sup>3</sup>*Unità CNISM di Salerno, Università degli Studi di Salerno, I-84084 Fisciano (SA), Italy*

<sup>4</sup>*Max-Planck-Institut für Festkörperforschung, Heisenbergstrasse 1, D-70569 Stuttgart, Germany*

<sup>5</sup>*Marian Smoluchowski Institute of Physics, Jagiellonian University, prof. Łojasiewicza 11, PL-30348 Kraków, Poland*

(Dated: November 12, 2015)

We elucidate the effects of defect disorder and  $e$ - $e$  interaction on the spectral density of the defect states emerging in the Mott-Hubbard gap of doped transition-metal oxides, such as  $\text{Y}_{1-x}\text{Ca}_x\text{VO}_3$ . A soft gap of kinetic origin develops in the defect band and survives defect disorder for  $e$ - $e$  interaction strengths comparable to the defect potential and hopping integral values above a doping dependent threshold, otherwise only a pseudogap persists. These two regimes naturally emerge in the statistical distribution of gaps among different defect realizations, which turns out to be of Weibull type. Its shape parameter  $k$  determines the exponent of the power-law dependence of the density of states at the chemical potential ( $k - 1$ ) and hence distinguishes between the soft gap ( $k \geq 2$ ) and the pseudogap ( $k < 2$ ) regimes. Both  $k$  and the effective gap scale with the hopping integral and the  $e$ - $e$  interaction in a wide doping range. The motion of doped holes is confined by the closest defect potential and the overall spin-orbital structure. Such a generic behavior leads to complex non-hydrogen-like defect states that tend to preserve the underlying  $C$ -type spin and  $G$ -type orbital order and can be detected and analyzed via scanning tunneling microscopy.

PACS numbers: 75.25.Dk, 68.35.Dv, 71.10.Fd, 71.55.-i

Defects in semiconductors and insulators determine their transport properties and are responsible for their usefulness for electronics. The hopping between defect states depends on their relative energy and is largely a function of disorder. In case of small hopping amplitudes, the long-range  $e$ - $e$  interaction becomes extremely relevant as it modifies substantially the energy of defect states and their occupations. In a seminal work [1, 2], it was shown that a soft gap develops in the density of states (DOS),  $N(\omega) \propto |\omega|^\kappa$  with exponent  $\kappa = d - 1$  for system dimension  $d = 2, 3$ , in the classical Coulomb glass model: it is known as Coulomb gap [3]. Further theoretical [4–6] and experimental [7] studies confirmed the remarkable success of the strong coupling approach for defects.

We consider defects in a quite different class of compounds: Mott insulators exhibiting a Mott-Hubbard (MH) gap due to short-range  $e$ - $e$  interactions [8] that separates the lower Hubbard band (LHB) from the upper Hubbard band (UHB) [9]. Defects in Mott insulators feature many fascinating behaviors [10–16] and are usually thought to lead to only two alternatives: either the MH gap collapses or the defect states inside the gap undergo an Anderson transition, as proposed by Mott [17] for  $\text{La}_{1-x}\text{Sr}_x\text{VO}_3$  and for the high- $T_c$  cuprates. However, why the insulator-to-metal transition occurs in vanadates at much higher doping than in cuprates, although in both systems the MH bands do not disappear with metalization [18, 19], is still not understood. Then, instead from the Anderson-Hubbard model that features only short-range Hubbard-like interactions and one orbital flavor [20–24], we start from an extended Hubbard model with long-range  $e$ - $e$  interactions, which allows us to study the effect of the self-consistent screening of defect potentials, and 3 orbital flavors. It provides a platform for describing the spin-orbital correlations of the perovskite vanadates, such as  $\text{Y}_{1-x}\text{Ca}_x\text{VO}_3$ , with

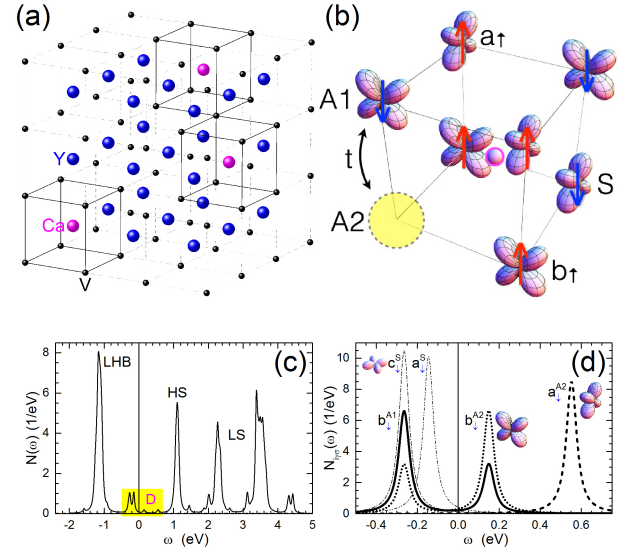


FIG. 1. (color online) (a)  $\text{Y}_{1-x}\text{Ca}_x\text{VO}_3$  lattice with a random distribution of Ca defects. (b) A Ca defect in the center of a cube made of 8 V ions. The related hole (yellow circle) is confined to move (hopping  $t$ ) along a vertical bond: the active  $\langle A1, A2 \rangle$  bond. The occupied  $a/b$  orbitals and spin states obey  $C$ -AF spin and  $G$ -AO order [19] on spectator (S) sites. (c) The LHB and the high-spin/low-spin (HS/LS) states of the UHB for a periodic arrangement of defects and  $x = 2\%$ . The defect states D (yellow rectangle) are located within the MH gap for  $V_D = 1.0$  eV and  $t = 0.2$  eV. (d) The zoom of the defect states D uncovers the contributions of the active bond and spectator sites (heavy and thin lines) and the formation of the kinetic gap.

active  $\{yz, zx\}$  orbitals at  $\text{V}^{3+}(xy)^1(yz/zx)^1$  ions, and co-existing  $C$ -type antiferromagnetic ( $C$ -AF) spin and  $G$ -type alternating orbital ( $G$ -AO) order [25], see Figs. 1(a) and (b).

The motion of a doped hole is bound to the charged Ca defect [Fig. 1(b)] and is further controlled by the underlying spin-orbital structure: it forms a localized spin-orbital polaron [26, 27]. Figure 1(c) displays the associated defect states in the MH gap in the case of a periodic arrangement of defects or, equivalently, of a short-range defect potential [28], and it also reveals the multiplets in the UHB. Due to the  $CG$  spin-orbital order, holes tend to form dimer states on specific  $c$ -bonds, the *active* bonds, which results in the formation of a kinetic gap, see Fig. 1(d). Our main goal is to understand whether this kinetic gap survives the potential fluctuations of random defects with long-range Coulomb potentials and which role the screening due to the  $t_{2g}$  electrons plays.

Crucial to our analysis are the electron-defect ( $V_{im}^D$ ) and the  $e$ - $e$  ( $V_{ij}$ ) interactions, both screened by the background dielectric constant  $\epsilon_c$  due to core electrons (no  $t_{2g}$  electrons),

$$V_{im}^D = v(R_{im}), \quad V_{ij} = \eta v(r_{ij}), \quad v(r) = \frac{e^2}{\epsilon_c r}, \quad (1)$$

where  $R_{im}$  and  $r_{ij}$  stand for the electronic distances between the V ion at site  $i$  and the Ca defect at site  $m$  and between two V ions at sites  $i$  and  $j$ , respectively. The typical binding energy of a hole is  $V_D = V^D(d) \approx 1$  eV [19], where  $d$  is the distance between the defect and its closest V ions and  $\epsilon_c \simeq 5$ . A hole would propagate along the  $c$  axis at  $V_D = 0$  [29], similar to an  $e_g$  hole in  $Y_{2-x}Ca_xBaNiO_6$  [30].

The Hamiltonian of the doped  $Y_{1-x}Ca_xVO_3$  reads as

$$\begin{aligned} \mathcal{H}_{t_{2g}} = & \sum_{im} V_{im}^D n_i + \sum_{i \neq j} V_{ij} n_i n_j + \mathcal{H}_{CF} + \mathcal{H}_{JT} \\ & - \sum_{\langle ij \rangle \sigma \alpha} t_{ij}^\alpha (d_{i\sigma\alpha}^\dagger d_{j\sigma\alpha} + \text{H.c.}) + \mathcal{H}_{loc}(U, J_H), \quad (2) \end{aligned}$$

where  $n_i = \sum_{\sigma\alpha} n_{i\sigma\alpha}$  and  $n_{i\sigma\alpha} = d_{i\sigma\alpha}^\dagger d_{i\sigma\alpha}$ , with orbital flavor  $\alpha \in \{a, b, c\}$  standing for  $a \equiv yz$ ,  $b \equiv zx$ ,  $c \equiv xy$ . The 1<sup>st</sup> two terms in Eq. (2) basically resemble the Coulomb glass model [1, 2] with site energies determined by the (random) positions of defects. The  $e$ - $e$  interaction  $V_{ij}$  plays a major role in determining the occupation of these states as for  $\eta = 1$  the combined defect-hole potential is dipolar [31], while for  $\eta = 0$  it is monopolar.  $V_{ij}$  is also responsible for the additional screening involving the transitions between the Hubbard bands and the defect states. Further terms in the 1<sup>st</sup> line,  $\mathcal{H}_{CF} = -\Delta_c \sum_{i\sigma} n_{i\sigma c}$  and  $\mathcal{H}_{JT}$ , denote the crystal-field and Jahn-Teller terms for the  $t_{2g}$  electrons [28]. A new dimension of the defect problem arises from the 2<sup>nd</sup> line that includes the nearest-neighbor hopping (the symmetry of  $t_{2g}$  orbitals implies that  $t_{ij}^\alpha$  is equal to  $t$  and different from 0 only for a bond  $\langle ij \rangle$  direction different from  $\alpha$  [32–34]), and the local Hubbard physics of the triply degenerate  $t_{2g}$  electrons,  $\mathcal{H}_{loc}(U, J_H)$  [35]. The local Coulomb interactions include intraorbital Hubbard  $U$  and Hund's exchange  $J_H$  expressed in the SU(2) invariant form [36]. They are responsible for the multiplets in the UHB for  $d$ - $d$  charge excitations [Fig. 1(c)].

We solve the Hamiltonian (2) self-consistently employing the unrestricted Hartree-Fock (uHF) approximation [37].

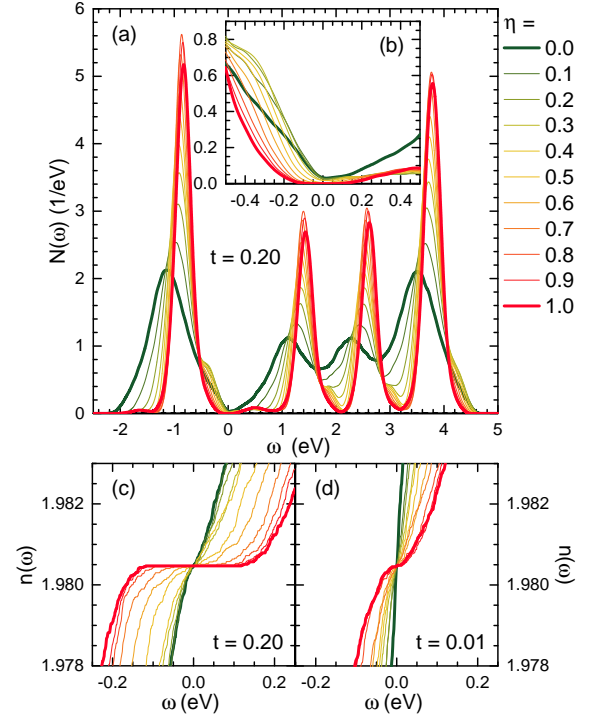


FIG. 2. (color online) (a) Density of states  $N(\omega)$  averaged over  $M = 100$  defect realizations for doping concentration  $x = 2\%$ ,  $t = 0.2$  eV, and for  $\eta \in [0, 1]$ . A Gaussian smearing of 0.03 eV has been used. Inset (b) shows a zoom of  $N(\omega)$  in (a) close to the Fermi energy ( $\omega = 0$ ). A zoom of the averaged integrated DOS  $n(\omega)$  close to Fermi energy is shown for: (c)  $t = 0.2$  eV, and (d)  $t = 0.01$  eV.

There are two main advantages of the uHF approach we like to emphasize: (i) uHF reproduces the Hubbard bands and the multiplet splitting not only for undoped systems [37], but also in presence of defects [27] and orbital polarization and SU(2) rotation [28]; (ii) the spatial distribution and the occupation of each defect state depends on all other occupied states in presence of disorder and long-range interactions (1). As a matter of fact, uHF solves this central and complex optimization problem in the most efficient way. The derivation of the uHF equations is standard; more details can be found, for instance, in Refs. [27, 28]. We present results obtained for a cluster of  $N_a = 8 \times 8 \times 8$  V ions with periodic boundary conditions, after averaging over  $M = 100$  statistically different Ca defect realizations. We use the standard parameters for  $YVO_3$ , i.e.,  $U = 4.0$  eV,  $J_H = 0.6$  eV,  $\Delta_c = 0.1$  eV [28].

The  $2_{\text{spin}} \times 3_{\text{orbital}} \times N_a$  uHF eigenvalues  $\epsilon_{s,l}$  obtained for a given defect realization  $s$  yield the averaged DOS per V ion,

$$N(\omega) = \frac{1}{M} \sum_{s=1}^M \left[ \frac{1}{N_a} \sum_{l=1}^{6N_a} \delta(\omega + \mu_s - \epsilon_{s,l}) \right]. \quad (3)$$

The Fermi energy  $\mu_s$  not only separates the occupied from the unoccupied states in each defect realization  $s$ , but as well reflects, via the energy optimization, a repulsion between such states as in the Peierls effect [38]. Therefore, the average over

different defect realizations calls for an overall alignment of the energy scales by means of the different  $\mu_s$ .

Figure 2 displays the variation of the MH multiplets for different strengths of  $e$ - $e$  interaction, encoded by the parameter  $\eta$ , for doping  $x = 2\%$  of random Ca defects (i.e., for 10 defects) [cf. Figs. 1(c) and (d) for a periodic arrangement of defects]. The electronic states close to the defects are pushed by the potential  $V_D$  away from the LHB into the MH gap. However, the actual energy distribution of defect states is strongly dependent on the screening of the  $t_{2g}$  electrons via the  $e$ - $e$  interaction and a soft gap gradually opens up in the DOS on increasing  $\eta$ . The inset (b) clearly shows the non-monotonous variation of the defect states inside the MH gap on varying the screening. On the large energy scale, two important changes occur when  $\eta$  is varied. For  $\eta = 0$ , the defect potential is unscreened and the interaction with further randomly distributed defects broadens the Hubbard bands. For  $\eta = 1$ , the screening is instead complete: each defect forms an exciton with a doped hole and the resulting interaction between excitons is dipolar with a tremendous suppression of the effects of disorder and a dramatic narrowing of the Hubbard bands.

To analyze the behavior of the soft gap in  $N(\omega)$  without suffering from the unavoidable smearing, we discuss next the averaged integrated DOS,  $n(\omega) = \int_{-\infty}^{\omega} d\omega' N(\omega')$ , in the vicinity of the Fermi energy and the related plateau [see Figs. 2(c) and (d)]. It is worth noting the following key features in  $n(\omega)$ : (i) there is an evident gap/plateau for  $t = 0.2$  eV (being a typical value for cubic vanadates [32]) and  $\eta = 1$ , but not for small  $t = 0.01$  eV, and (ii) on decreasing the screening  $\eta \rightarrow 0$ , the gap/plateau disappears even for  $t = 0.2$  eV.

In order to establish the statistical behavior of  $N(\omega)$  in the limit  $M \rightarrow \infty$ , we use that  $N(\omega)$  is proportional to the probability distribution function  $P^*(\omega)$  that a state in a generic defect realization has energy  $\omega$  relative to its Fermi energy  $\mu_s$ . Then, we find that a generic defect realization features a gap of size  $E$  with a probability governed by a Weibull probability distribution function,

$$P(E) = \theta(E - \zeta) \frac{k}{\lambda} \left( \frac{E - \zeta}{\lambda} \right)^{k-1} e^{-\left( \frac{E - \zeta}{\lambda} \right)^k}, \quad (4)$$

with shape parameter  $k$ , scale parameter  $\lambda$  and location parameter  $\zeta$ . Accordingly, if  $\zeta = 0$ , we have  $P^*(\omega) = \frac{k}{\lambda^k} |\omega|^{k-1}$  and  $N(\omega) \propto |\omega|^{k-1}$  both for  $|\omega| \ll \lambda$ , that is we have a soft gap for  $k \geq 2$ , a pseudogap for  $1 < k < 2$  and no gap for  $k = 1$ . Instead, if  $\zeta > 0$ , we have  $N(\omega) = 0$  for  $|\omega| \leq \zeta$  and  $N(\omega) \propto (|\omega| - \zeta)^{k-1}$  for  $\zeta < |\omega| \ll \lambda$ , that is we have a hard gap. Thus,  $P(E)$  results in a robust scheme to determine the behavior of  $N(\omega)$  close to the Fermi energy, that is the presence and type of gap in the system. The numerical data obtained for the gaps of  $M$  defect realizations for  $t = 0.2$  (0.01) eV and  $\eta = 0$  and 1 are compared in Figs. 3(a) and (b) to the corresponding statistical least-squares fits to  $P(E)$ . The fits are indeed excellent in all cases and give systematically  $\zeta = 0$ .

In Fig. 3(c), we report the  $n(\omega)$  curves of Fig. 2(c) successfully reconstructed with the help of  $P(E)$ . The plateau/gap  $\Delta$

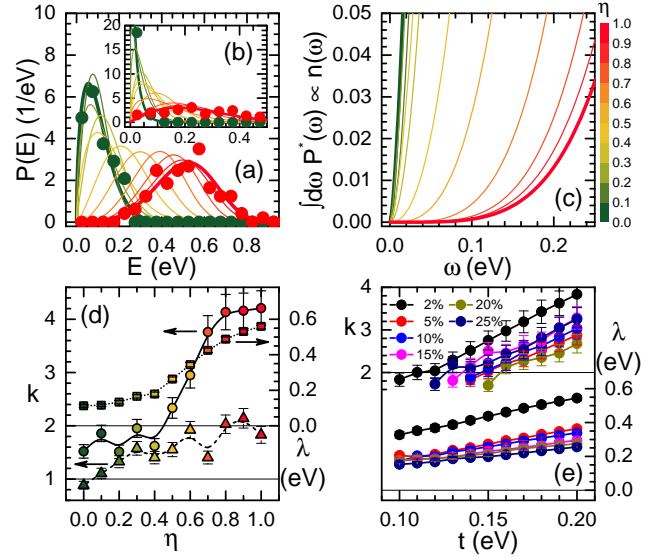


FIG. 3. (color online) (a)  $P(E)$  for  $t = 0.2$  eV and different values of  $\eta$  (colors as in Fig. 2). Lines are least-squares fits from Eq. (4) and dots are numerical data for  $\eta = 0$  and 1 computed from the  $M$  defect realizations; inset (b) same as (a) but for  $t = 0.01$  eV; (c) averaged integrated DOS  $n(\omega)$  calculated from (4); (d)  $\eta$  dependence of  $k$  and  $\lambda$  for  $t = 0.2$  eV (circles and squares, respectively) and for  $t = 0.01$  eV (only  $k$  with triangles); (e)  $t$  dependence of  $k$  and  $\lambda$  for doping  $x = 2, 5, 10, 15, 20$  and 25% at  $\eta = 1$ . Lines in (d) and (e) are guides to the eye.

present in Fig. 2(c) for  $\eta \geq 0.5$  is due to the finiteness of  $M$ : its statistical value is  $\Delta \doteq \lambda / \sqrt[k]{M}$  that vanishes for  $M \rightarrow \infty$ . Figures 3(d) and 3(e) summarize the dependence of  $k$  and  $\lambda$  on the  $e$ - $e$  interaction strength  $\eta$  and  $t$ , respectively. Both  $k$  and  $\lambda$  increase with increasing  $e$ - $e$  interaction  $\eta$ , see Fig. 3(d). At  $t = 0.2$  eV, for  $\eta > 0.5$ , we have  $k > 2$  and, therefore, a soft gap. On the contrary, for  $t = 0.01$  eV,  $k < 2$  is found for all values of  $\eta$ : the  $e$ - $e$  interaction alone is not sufficient to stabilize a gap and only a pseudogap persists. It is worth noting the almost linear increase of both  $k$  and  $\lambda$  with increasing  $t$  shown at  $\eta = 1$  in Fig. 3(e), which justifies calling the soft gap a kinetic gap. We also observe a rather slow, but monotonous, decrease of  $\lambda$  on increasing the doping  $x$ . The most important feature is the non-universality of the exponent  $k$  that scales with both  $\eta$  and  $t$ , and is not simply given by the system dimensionality, in contrast to the Coulomb gap in disordered semiconductors [1, 2].

The kinetic gap formation is triggered by the doped holes that do not form symmetric, hydrogen-like, orbitals around the defects. Instead, due to the interplay with the spin-orbital order, they form composite spin-orbital polarons that localize in a symmetry broken form on *active* bonds. Which of the 4 closest  $c$ -bonds of a defect is chosen depends on the interactions with all other defects. To detect and analyze these complex defects, we study in the following the scanning tunneling microscopy (STM) patterns [39–42] that correspond here to the spatially resolved spin-orbital ( $\sigma\alpha$ ) DOS integrated from the



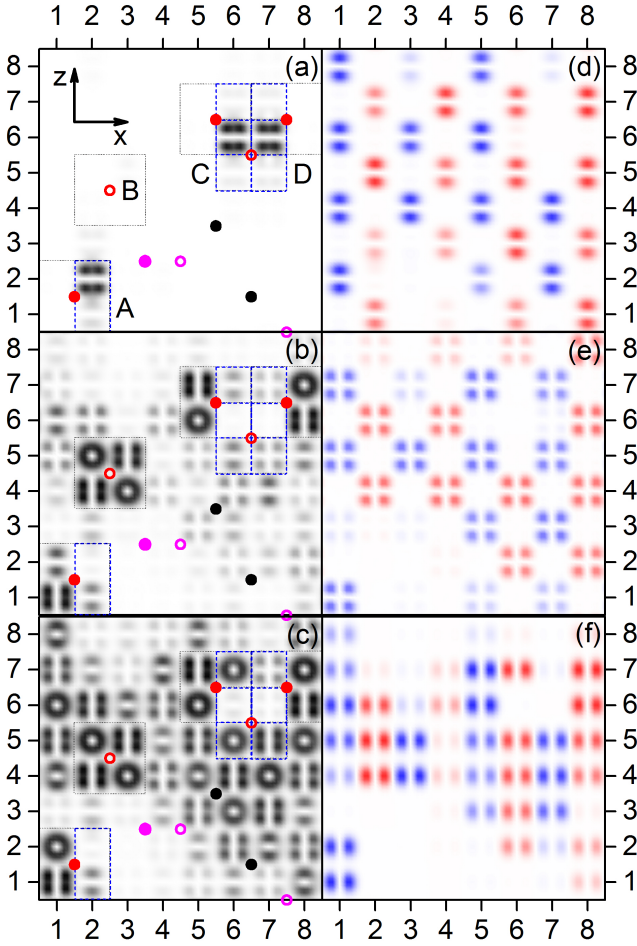


FIG. 4. (color online) Integrated electron/hole density  $\rho_{\sigma\alpha}(x, y, z; V)$  in the  $ac$  plane with  $y = 1$  [V ions are at  $(x, 1, z)$  sites] for a typical defect realization at  $x = 2\%$ ,  $\eta = 1$ , and  $t = 0.2$  eV. The defects closest to the shown plane at  $y = 1.5$  (0.5) are marked by red dots (circles), at  $y = 2.5$  (7.5) by magenta dots (circles) and more distant ones by black dots. Faces of V cubes hosting a defect are indicated by thin gray dotted lines, while *active* bonds by thick blue dashed lines. Panel (a) shows the integrated unoccupied density at  $V = 1.0$  eV, with defect features A, B, C, D discussed in the text; panels (b) and (c) show the integrated occupied density at: (b)  $V = -0.7$  eV, (c)  $V = -0.8$  eV. Right panels show the spin-orbital partial densities at  $V = -0.8$  eV for: (d)  $a = yz$ , (e)  $b = xz$ , and (f)  $c = xy$  orbitals. Red (blue) color for up (down) spin projections clearly show  $C$ -AF order.

Fermi energy to the applied voltage  $V$  for a particular defect realization  $s$ ,  $\rho_{\sigma\alpha}(x, y, z; V) = |\int_0^V d\omega \rho_{\sigma\alpha}(x, y, z; \omega + \mu_s)|$ .

The integrated unoccupied density pattern summed over all spin-orbital degrees of freedom,  $\sum_{\sigma\alpha} \rho_{\sigma\alpha}(x, y, z; V)$ , is shown in Fig. 4(a) for  $V = 1.0$  eV. In the lower left corner, we recognize an unoccupied defect state (A) at coordinates  $(x, y, z) = (2, 1, z)$  with a finite hole density at vanadium sites  $z = 1, 2$  (on the *active* bond). The asymmetry relative to its closest Ca defect at  $(1.5, 1.5, 1.5)$  is evident. The degree of orbital polarization, i.e., increased weight at  $z = 2$ , is due to the other defects and the Jahn-Teller potential. Fig. 4(b)

shows the occupied density for  $V = -0.7$  eV. Close to the same defect at  $(1.5, 1.5, 1.5)$ , we see two occupied  $c$ -bonds: one at  $(1, 1, 1\&2)$  with two electrons per site (*spectator* sites), and another one at  $(2, 1, 1\&2)$  — the *active* bond (A), with a single hole fluctuating in an asymmetric way along the bond parallel to the  $c$  axis. The defect (B) has its hole on a neighbor  $y$ -plane and we see only *spectator* sites. (C) and (D) mark a pair of *active* bonds belonging to three V cubes hosting three defects. More defect states appear at  $V = -0.8$  eV [Fig. 4(c)] that are not well separated from the LHB. Here the complexity of the defect landscape is apparent as well as the interaction of the doped holes with the spin-orbital background.

The landscapes in Figs. 4(d-f) represent the partly occupied spin-orbital densities  $\rho_{\sigma\alpha}(x, y, z; V)$  of defect states at  $V = -0.8$  eV. The red/blue stripe structure for up (down) spins reveals that both the underlying  $C$ -AF spin order and the  $G$ -AO order survive the doping by charge defects, in contrast to what happens in high- $T_c$  cuprates where the spin order of the parent compound is destroyed [43, 44]. This supports the findings of the Tokura's group that  $C$ -AF/ $G$ -AO order is preserved in various doped vanadate systems [19].

Summarizing, we have shown that charged defects in vanadates generate an intrinsic kinetic gap within the Mott-Hubbard gap that survives defect disorder for strong  $e$ - $e$  interactions implying a strong dielectric screening. The kinetic gap transforms into a soft gap with power-law dependence:  $N(\omega) \propto |\omega|^{k-1}$ . We have established that the exponent  $k$  is non-universal and scales with both the kinetic scale  $t$  and the  $e$ - $e$  interaction strength  $\eta$ . We suggest that an STM analysis can provide highly valuable microscopic information on the complex non-hydrogen-like states of doped holes, but this remains an experimental challenge.

We thank A. Rost and H. Shinaoka for insightful discussions. A.A. acknowledges kind hospitality at Max-Planck-Institut für Festkörperforschung, Stuttgart. A.M.O. kindly acknowledges support by Narodowe Centrum Nauki (NCN, National Science Center) Project No. 2012/04/A/ST3/00331.

- 
- [1] A.L. Efros and B.I. Shklovskii, J. Phys. C **8**, L49 (1975).
  - [2] A.L. Efros, J. Phys. C **9**, 2021 (1976).
  - [3] M. Pollak, Phil. Mag. B **65**, 657 (1992).
  - [4] F. Epperlein, M. Schreiber, and T. Vojta, Phys. Rev. B **56**, 5890 (1997).
  - [5] M. Müller and L.B. Ioffe, Phys. Rev. Lett. **93**, 256403 (2004).
  - [6] A.L. Efros, B. Skinner, and B.I. Shklovskii, Phys. Rev. B **84**, 064204 (2011); B. Skinner, T. Chen, and B.I. Shklovskii, Phys. Rev. Lett. **109**, 176801 (2012).
  - [7] V.Yu. Butko, J.F. DiTusa, and P.W. Adams, Phys. Rev. Lett. **84**, 1543 (2000).
  - [8] M. Imada, A. Fujimori, and Y. Tokura, Rev. Mod. Phys. **70**, 1039 (1998).
  - [9] H. Eskes, M.B.J. Meinders, and G.A. Sawatzky, Phys. Rev. Lett. **67**, 1035 (1991); M.B.J. Meinders, H. Eskes, and G.A. Sawatzky, Phys. Rev. B **48**, 3916 (1993).
  - [10] W. Brzezicki, A.M. Oleś, and M. Cuoco, Phys. Rev. X **5**,

- 011037 (2015); arXiv:1506.07048 (2015).
- [11] T. Tanaka, M. Matsumoto, and S. Ishihara, Phys. Rev. Lett. **95**, 267204 (2005).
  - [12] K.W. Kim, J.S. Lee, T.W. Noh, S.R. Lee, and K. Char, Phys. Rev. B **71**, 125104 (2005).
  - [13] C. Şen, G. Alvarez, and E. Dagotto, Phys. Rev. Lett. **105**, 097203 (2010).
  - [14] J.-Q. Yan, J.-S. Zhou, J.G. Cheng, J.B. Goodenough, Y. Ren, A. Llobet, and R.J. McQueeney, Phys. Rev. B **84**, 214405 (2011).
  - [15] N. Pavlenko, T. Kopp, E.Y. Tsymbal, G.A. Sawatzky, and J. Mannhart, Phys. Rev. B **85**, 020407(R) (2012); N. Pavlenko, T. Kopp, E.Y. Tsymbal, J. Mannhart, and G.A. Sawatzky, *ibid.* **86**, 064431 (2012).
  - [16] H.O. Jeschke, J. Shen, and R. Valenti, New J. Phys. **17**, 023034 (2015).
  - [17] N.F. Mott, J. Phys. (France) **50**, 2811 (1989).
  - [18] P. Abbamonte, A. Rusydi, S. Smadici, G.D. Gu, G.A. Sawatzky, and D.L. Feng, Nat. Phys. **1**, 155 (2005).
  - [19] J. Fujioka, S. Miyasaka, and Y. Tokura, Phys. Rev. B **77**, 144402 (2008).
  - [20] D. Belitz and T.R. Kirkpatrick, Rev. Mod. Phys. **66**, 261 (1994).
  - [21] H. Shinaoka and M. Imada, J. Phys. Soc. Jpn. **78**, 094708 (2009).
  - [22] V. Dobrosavljević and G. Kotliar, Phys. Rev. Lett. **78**, 3943 (1997); M.C.O. Aguiar, V. Dobrosavljević, E. Abrahams, and G. Kotliar, *ibid.* **102**, 156402 (2009).
  - [23] Yun Song, R. Wortis, and W.A. Atkinson, Phys. Rev. B **77**, 054202 (2008).
  - [24] M. Sawicki, D. Chiba, A. Korbecka, Y. Nishitani, J.A. Majewski, F. Matsukura, T. Dietl, and H. Ohno, Nat. Phys. **6**, 22 (2010); C. Śliwa and T. Dietl, Phys. Rev. B **83**, 245210 (2011).
  - [25] J. Fujioka, T. Yasue, S. Miyasaka, Y. Yamasaki, T. Arima, H. Sagayama, T. Inami, K. Ishii, and Y. Tokura, Phys. Rev. B **82**, 144425 (2010).
  - [26] K. Wohlfeld, A.M. Oleś, and P. Horsch, Phys. Rev. B **79**, 224433 (2009).
  - [27] P. Horsch and A.M. Oleś, Phys. Rev. B **84**, 064429 (2011).
  - [28] A. Avella, P. Horsch, and A.M. Oleś, Phys. Rev. B **87**, 045132 (2013).
  - [29] S. Ishihara, Phys. Rev. Lett. **94**, 156408 (2005).
  - [30] E. Dagotto, J. Riera, A. Sandvik, and A. Moreo, Phys. Rev. Lett. **76**, 1731 (1996).
  - [31] Except for the monopolar interaction with the closest defect.
  - [32] G. Khaliullin, P. Horsch, and A.M. Oleś, Phys. Rev. Lett. **86**, 3879 (2001); Phys. Rev. B **70**, 195103 (2004).
  - [33] A.B. Harris, T. Yildirim, A. Aharony, O. Entin-Wohlman, and I.Y. Korenblit, Phys. Rev. Lett. **91**, 087206 (2003).
  - [34] M. Daghofer, K. Wohlfeld, A.M. Oleś, E. Arrigoni, and P. Horsch, Phys. Rev. Lett. **100**, 066403 (2008); P. Wróbel and A.M. Oleś, *ibid.* **104**, 206401 (2010).
  - [35] M. Daghofer, A. Nicholson, A. Moreo, and E. Dagotto, Phys. Rev. B **81**, 014511 (2010).
  - [36] A.M. Oleś, Phys. Rev. B **28**, 327 (1983).
  - [37] T. Mizokawa and A. Fujimori, Phys. Rev. B **54**, 5368 (1996).
  - [38] P. Horsch and F. Mack, Eur. Phys. J. B **5**, 367 (1998).
  - [39] Øystein Fischer, M. Kugler, I. Maggio-Aprile, C. Berthod, and C. Renner, Rev. Mod. Phys. **79**, 353 (2007).
  - [40] J.I. Pascual, J. Gómez-Herrero, C. Rogero, A.M. Baró, D. Sánchez-Portal, E. Artacho, P. Ordejón, and J.M. Soler, Chem. Phys. Lett. **321**, 78 (2000).
  - [41] D.A. Muller, N. Nakagawa, A. Ohtomo, J.L. Grazul, and H.Y. Hwang, Nature (London) **430**, 657 (2004).
  - [42] M.J. Lawler, K. Fujita, J. Lee, A.R. Schmidt, Y. Kohsaka, C.K. Kim, H. Eisaki, S. Uchida, J.C. Davis, J.P. Sethna, and Eun-Ah Kim, Nature (London) **466**, 347 (2010).
  - [43] G. Khaliullin and P. Horsch, Phys. Rev. B **47**, 463 (1993).
  - [44] A. Avella, F. Mancini and R. Münzner, Phys. Rev. B **63**, 245117 (2001).